Arsenic sorption by red mud-modified biochar produced from rice straw

by Chuan, W., Huang, L., Xue, S., Hartley, W., Cui, M. and Wong, M.

DOI: https://doi.org/10.1007/s11356-017-9466-7

Chuan, W., Huang, L., Xue, S., Hartley, W., Cui, M. and Wong, M. 2017. Arsenic sorption by red mud-modified biochar produced from rice straw. *Environmental Science and Pollution Research*

20 June 2017

Arsenic sorption by red mud-modified biochar produced from rice straw

Chuan Wu[a], Liu Huang[a], Sheng-Guo Xue[a*], Li-Zheng Shi[a], William Hartley[b], Mengqian Cui[a], Ming-Hung Wong[c, d]

[a] *School of Metallurgy and Environment, Central South University, Changsha 410083, PR China*

[b] *Crop and Environment Sciences Department, Harper Adams University, Newport, Shropshire, TF10 8NB, United Kingdom*

[c] *Consortium on Health, Environment, Education and Research (CHEER), The Education University of Hong Kong,, Tai Po, Hong Kong Special Administrative Region, PR China*

[d] *School of Environment, Jinan University, Guangzhou, PR China*

[*] Corresponding author:

Tel: +86-13787148441. E-mail address: sgxue@csu.edu.cn.

Abstract

Rice straw biochar modified with red mud (RM-BC) is used here as an adsorbent to remove As from aqueous solutions. Rice straw is an agricultural waste material whilst red mud is a waste product from bauxite processing. SEM-EDS and XRD analyses demonstrated that red mud had distributed successfully on the surface of the rice straw biochar. With increasing solution pH, arsenate adsorbtion on RM-BC decreased whilst As(III) increased. Arsenate adsorption kinetics on RM-BC fitted the pseudo-second-order model, whilst that of As(III) favored the Elovich model. All sorption isotherms produced superior fits with the Langmuir model. RM-BC exhibited improved As removal capabilities, with a maximum adsorption capacity (Qmax) for As(V) of 5923 ug•g-1, approximately ten times greater than that of the untreated BC (552.0 ug•g-1). Furthermore, X-ray absorption near-edge spectroscopy (XANES) indicated that adsorption of As(V) on RM-BC was possibly due to surface complexation and electrostatic interactions. RM-BC may be used as a valuable adsorbent for removing As due to the waste materials being relatively abundant.

Keywords: Biochar; Red mud; Pyrolysis; Arsenic; XANES

1. Introduction

Arsenic (As) has been recognized as ‘a known carcinogen’ by the World Health Organization (WHO) (WHO, 2001). Many anthropogenic activities including the use of insecticides, herbicides and phosphate fertilizers, semi-conductor industries, mining and smelting operations, industrial processes, coal combustion and timber preservatives have released As into soils and groundwater causing global concern (Kim et al., 2014; Yu et al., 2015). Arsenic-contaminated soils are harmful to food safety and groundwater quality, and eventually threaten human health in many regions of the world such as Mexico, USA, China, Bangladesh and Pakistan (Jadhav et al., 2015; Wu et al., 2016a). In soil, As compounds exist either as inorganic and organic species. Generally, inorganic As species (arsenite As(III) and arsenate As(V)) are more toxic than organic forms to living organisms (Beesley et al., 2014).

Red mud (RM) is an alkaline waste by-product generated from the extraction of alumina from bauxite during the Bayer process. Due to the very large volumes of red mud (120 million tons per year) and difficulty with its disposal, it is essential to find alternative options for its treatment and use (Klauber et al., 2011). Generally, the mineralogical composition of red mud consists of various forms of iron and aluminum oxides, calcium and sodium aluminum silicates and numerous titanium compounds. Red mud has a fine, porous structural nature and its surface carries significant hydroxyl groups (Liu and Naidu, 2014). As a result, the material has great potential to

remediate As contamination both in soils and groundwater (Altundogan, 2000; Klauber et al., 2011; Lopes et al., 2013). Previous studies confirmed that red mud, or neutralized red mud, can remove As from aqueous solutions (Altundogan, 2000; Genc, 2003). Furthermore, it has been demonstrated that RM can influence As fractionation in soils (Lee et al., 2011; Yan et al., 2013). The interaction mechanisms between As and red mud can be mainly attributed to electrostatic attraction/repulsion, chemical interaction (Castaldi et al., 2010; Wu et al., 2016b; Rubinos et al., 2005).

Biochar is a stable solid produced by thermal or hydrothermal conversion of carbonaceous biomass under oxygen-limiting conditions (Zhang et al., 2013). It has been used in numerous applications mostly as a soil amendment/conditioner, a waste management tool and to mitigate global warming (Ahmad et al., 2014). Furthermore, biochar may improve soil fertility, increase soil nutrient bioavailability, improve agricultural productivity and sequester carbon (Lone et al., 2015). Nevertheless it has been shown that biochar may also reduce the bioavailability of essential plant micronutrients (Hartley, 2016). Additionally, biochar can effectively remove water contaminants (such as As, Cr and Cd) because of its favorable physicochemical properties (large surface area and porous structure) (Tan et al., 2016). It has also been reported that the characteristics of biochar, mainly the large surface area and cation exchange capacity (CEC), can lead to the stabilization of many heavy metals in the environment (Gregory et al., 2014).

Conversely, it has been demonstrated that biochar can elevate soil pH and thus mobilize As, which has limited its application in As remediation (Hartley et al., 2009;

Beesley et al., 2014). Recent studies have focused on the application of biochar-based materials, particularly biochar-based composites, that have enhanced capabilities as adsorbents for removing As from water and soils. Biochar-based materials such as $ZnCl_2$-activated biochar and Ca-/Fe-modified biochar were used to remove As (including As(III) and As(V)) in water (Samsuri et al., 2013; Xia et al., 2016). However, the preparation procedures for these materials are relatively complex and expensive.

Biochar has a porous structure that can be used to support the distribution of particles within its matrix (Wang et al., 2015a). Red mud shows some potential for As adsorption due to its distinctive oxide-rich constitution, especially iron and aluminum oxides, surface hydroxyl groups and its porous nature (Altundogan et al., 2000; Liu et al., 2011). Both rice straw and red mud are low cost, abundant materials. However, there seems to be a lack of information on the use of biochar for As remediation, when compared with other metals (Beesley et al., 2014). Based on this evidence, the study attempts to develop a novel red mud-modified biochar, in order to (1) characterize its physicochemical properties; (2) compare the kinetics of As sorption by red mud-modified biochar and untreated biochar produced from rice straw; and (3) investigate adsorption mechanisms using X-ray absorption spectroscopy (XANES).

2. Materials and methods

2.1. Materials

All chemicals used in this study were analytical grade. Deionized water was used to prepare all solutions. Sodium arsenite ($NaAsO_2$) and sodium arsenate ($Na_2HAsO_4 \cdot 12H_2O$) were purchased from Aldrich Chemical Co.

Rice straw was collected from a paddy field located around Central South University (Hunan, P.R. China). It was milled into a powder (0.15 mm) then used for biochar production (Chang et al., 2014). Red mud (RM), obtained from the Guangxi Pingguo alumina refinery (Pingguo, Guangxi Province, China), was oven-dried overnight at 60 °C.

2.2. Biochar preparation

Red mud-modified biochar (RM-BC) was produced using the method adopted by Wang et al. (2015a) and Yao et al. (2014). Approximately 2 g of RM at its natural pH was added to 500 mL deionized water and stirred for 30 min with a Magnetic Stirrer (85-2, Zhongda instrument corporaion in Jintan) to obtain stable RM suspensions. Subsequently, 10 g of rice straw was thoroughly mixed with the RM suspension and the mixture stirred for 2 h. Finally, the RM-modified feedstock was separated from the liquid by oven-drying at 80℃.

Pyrolysis of the RM-modified feedstock took place in a muffle furnace (SX_2-5-12,

133 Yuandong Therm corporaion in Changsha, China) at 600 ℃. In order to keep an
134 oxygen-free atmosphere during the pyrolysis process, oxygen-free N_2 was circulated
135 into the system at a flowrate of 200 mL/min. The temperature increased at a rate of
136 5 ℃/min until 600℃. The samples were pyrolyzed in the muffle furnace for 6 h. All
137 biochars were cooled to room temperature (25 ℃), washed with deionized water
138 several times to remove foreign substances, and oven dried at 80 ℃. Rice straw
139 without RM modification was prepared by the same process. Hereafter, red
140 mud-modified biochar and untreated biochar are named RM-BC and BC respectively.
141
142 *2.3. Material characterization*
143 The surface areas of BC and RM-BC were obtained using N_2 sorption on a
144 Monosorb surface area analyzer and calculated using the Brunauer–Emmett–Teller
145 (BET) method. Surface morphology of the each biochar was examined using a
146 scanning electron microscope, equipped with energy dispersive X-ray spectroscopy
147 (SEM, Phenom XL). Furthermore, the crystal structure of these materials was
148 characterized by X-ray powder diffraction (XRD, D/max 2550 VB+X).
149
150 *2.4. The effects of solution pH on adsorption*
151 Two stock solutions of 1000 mg/L As(III) and As(V) were prepared by dissolving
152 $NaAsO_2$ and $Na_2HAsO_4 \cdot 12H_2O$ in deionized water, respectively. Working solutions
153 (10 mg/L As(V) and 10mg/L As(III)) were prepared by diluting stock solutions with
154 deionized water. The working solutions contained 0.01 M NaCl to maintain a constant

ionic strength. pH was adjusted to 2, 4, 6, 8, 10 and 12 respectively, using 0.1 $mol \cdot L^{-1}$ HCl/NaOH. Approximately 0.12 g of BC or RM-BC was added to 30 mL As(V)/As(III) working solutions of the different pH values to make 4 $g \cdot L^{-1}$ concentrations. Subsequently these samples were shaken at a constant temperature (25 ±1 ℃) in an oscillator bath (DDHZ-300, Experimental facility corporation in TaiCang) at 200 rpm/min for 24h. Samples were then immediately passed through syringe membrane filters (0.45 mm) to determine As concentrations. Total As in the filtrate was measured by hydride generation atomic fluorescence spectrometry (HG-AFS, AFS-8230). The adsorbed concentration q ($\mu g\ g^{-1}$) of arsenate and arsenite was estimated as follows (Zhang et al., 2016):

$$q = \frac{(C_0 - C_t)V}{m}$$

Where q ($\mu g\ g^{-1}$) is the concentration of As(V)/As(III) adsorbed at equilibrium; C_0 and C_t ($\mu g\ L^{-1}$) are the initial and equilibrium solute concentrations individually; V (L) is the solute volume and m (g) is the adsorbents mass.

2.5. Adsorption kinetics

Prior to the study, it was observed that adsorption of As(V) and As(III) was most effective between 6 to 10 on BC and 2 to 10 on RM-BC. To investigate As adsorption mechanisms, adsorption kinetic studies were carried out at room temperature (25± 1℃). Approximately 0.12 g (4 $g \cdot L^{-1}$) of BC and RM-BC were added to 30 mL of As(V)/As(III) solutions (with concentrations of 10 $mg \cdot L^{-1}$). The solutions were then shaken at 200 rpm at optimal pH for predetermined time intervals of 0.5, 1, 2, 4, 8, 12,

16 and 24 h respectively. Samples were removed from the shaker and the adsorbents immediately separated from the solution by filtration. Total As in the filtrate was determined by HG-AFS (AFS-8230, Beijing Jitian Instruments Co., China). All investigations were performed in triplicate.

Kinetics data for As(V) and As(III) were fitted with a pseudo-first-order model, pseudo-second-order kinetic model and the Elovich model to explain the adsorption process. The governing equations of the mathematical models are listed as follows:

pseudo-first-order: $$\frac{dq_t}{dt} = k_1(q_e - q_t) \quad (1)$$

pseudo-second-order: $$\frac{dq_t}{dt} = k_2(q_e - q_t)^2 \quad (2)$$

Elovich: $$\frac{dq_t}{dt} = \alpha \exp(-\beta q_t) \quad (3)$$

Intraparticle diffusion: $$q_t = K_d t^{\frac{1}{2}} + C \quad (4)$$

Where q_t and q_e (μg/g) are the concentrations of As adsorbed at t and equilibrium time respectively, and k_1 (h^{-1}), k_2 (g μg^{-1} h^{-1}) and k_d(μg g^{-1} $min^{-1/2}$) are the rate constants for the pseudo-first-order kinetic model, pseudo-second-order kinetic model and intraparticle diffusion respectively. C(μg g^{-1}) is the y-intercept. Initial adsorption rate is regarded as α (μg g^{-1}) and β (μg g^{-1}) the desorption constant.

2.6. Adsorption isotherms

Adsorption equilibrium isotherms for As adsorption on RM-BC and BC were measured at different initial As(V)/As(III) concentrations (1-50 mg/L). Equilibrium adsorption investigations were performed for 24h at optimal pH. Two adsorption isothermal models, Langmuir and Freundlich, were applied to describe adsorption

isotherms. Equations were expressed as follows:

Langmuir: $$q_e = \frac{q_m k_L C_e}{1 + K_L C_e}$$

Freundlich: $$q_e = K_F C_e^{\,n}$$

Where q_e ($\mu g \cdot g^{-1}$) is the adsorbed concentration of As at equilibrium; C_e ($mg \cdot L^{-1}$) is the equilibrium concentration of As; q_m ($\mu g \cdot g^{-1}$) denotes the maximum adsorption capacity and n is the heterogeneity parameter; K_L（$L \cdot mg^{-1}$）and K_F represent the constants of Langmuir and Freundlich respectively.

For the Langmuir model, equilibrium parameter (R_L), employed to determine whether adsorption is favorable or not, is as follows (Sun et al., 2015):

$$R_L = \frac{1}{1 + K_L C_0}$$

Where C_0 (mg L^{-1}) is the initial concentration of As and K_L (L mg^{-1}) is the Langmuir constant. The adsorption process is either unfavorable ($R_L > 1$), linear ($R_L = 1$), favorable ($0 < R_L < 1$) or irreversible ($R_L = 0$).

2.7. X-ray absorption spectroscopy analysis

The mechanism of As(V) sorption on RM-BC was investigated by X-ray absorption spectroscopy (XANES). For reference XANES spectra, all minerals (hematite, goethite, magnetite and gibbsite) were purchased from Sigma. Approximately 4 $g \cdot L^{-1}$ of each mineral was applied to 30 mL of As(V) solution (10 $mg \cdot L^{-1}$) for 24 h using 0.01 $mol \cdot L^{-1}$ NaCl to maintain ionic strength. After sorption, the suspension was centrifuged, washed twice with 0.01 $mol \cdot L^{-1}$ NaCl at pH 5.5, then washed with Ultrapure Water and subsequently freeze-dried (Fan et al., 2014).

X-ray absorption data were recorded at beamline BL14W at the Shanghai Synchrotron Radiation Facility (SSRF) with a Si(1 1 1) double crystal monochromator. The synchrotron was operated at 3.5 GeV and beam current around 150 - 210 mA (Guo et al., 2011). Data processing was performed using Athena IFEFFIT package and SixPack. Principal component analysis (PCA), target transformation (TT), and linear combination fitting (LCF) of XANES data were used to quantitatively determine As species.

2.8. Data Analysis

All data was analyzed in SPSS 23.0. Figures were created in Origin 9.0.

3. Results and discussion

3.1. Characterization

The BET N_2 surface areas of BC and RM-BC were 210.29 m^2/g and 186.95 m^2/g, respectively. There was a decrease in the surface area of the raw biomass treated with red mud, suggesting that red mud possibly covers the pores of the biochar, which is in accordance with other materials such as kaolinite modified biochar (Yao et al., 2014) and hematite modified biochar (Wang et al., 2015a).

The morphology images and EDX of RM and RM-BC are shown in Fig.1. The EDX spectrum and SEM confirmed that the surface of biochar was loaded with red mud. The EDX analysis of RM-BC revealed extra peaks for calcium, aluminum, titanium, sodium and iron, which are the elemental compositions of red mud when

compared to that of BC (Fig. 1b). The surface of RM-BC appeared smooth without adsorption (Fig. 1b) and then became coarser after the adsorption of As(V) (Fig. 1c) and As(III) (Fig. 1d). The EDS spectra analysis showed that As was coated on the surface of the RM-BC, demonstrating that adsorption had occurred (Fig. 1c and 1d).

The structures of RM-BC and BC were clearly different, when examined by X-ray powder diffraction (XRD). XRD analysis of the RM-BC revealed the presence of crystalline phases identified as hematite, magnetite, goethite, calcite, gibbsite and perovskite which were not detected in the crystalline phases of BC (Fig. 2). The results further confirmed that red mud had been successfully loaded on the surfaces of the biochar matrix.

3.2. Effect of pH

The effect of pH on As(V) and As(III) adsorbed by BC and RM-BC are presented in Fig.3.a and Fig.3.b, respectively. The amount of adsorbed As(V) (q, $\mu g \cdot g^{-1}$) decreased with increasing pH on RM-BC (Fig.3.a). The maximum adsorption density for As(V) at pH=2 was 1622.51 $\mu g \cdot g^{-1}$. Adsorption capacity of BC for As(V) increased with increasing pH from 2 to 6, but then decreased when the pH ranged from 6 to 12. The maximum adsorption of BC was q=481.61 $\mu g \cdot g^{-1}$ at pH=6. Biochar had a somewhat lower As(V) adsorption capacity, when compared to that of RM-BC.

The effects of pH on As(III) adsorption are presented in Fig.3.b. Clearly, BC and RM-BC showed similar trends on the pH-dependent adsorption curves. The quantity adsorbed increased with pH, increasing from 2 to 10, but when pH was elevated from

10 to 12, the adsorbed amount of both absorbents decreased. Overall, the results indicated that As(V) is adsorbed in acidic pH conditions, whilst As(III) tends to be adsorbed in alkaline environments. In addition, red mud modification significantly enhanced the sorption ability of biochar both on As(V) and As(III).

pH is considered as a crucial factor influencing As species distribution and the surface charge of BC/RM-BC. Anionic species of arseneous and arsenic acids are dictated by pH. Ionization equations are listed as follows (Wei et al., 2016):

$H_3AsO_3 \leftrightarrow H_2AsO_3^- + H^+$ $pKa_1 = 9.23$

$H_2AsO_3^- \leftrightarrow HAsO_3^{2-} + H^+$ $pKa_2 = 12.10$

$HAsO_3^{2-} \leftrightarrow AsO_3^{3-} + H^+$ $pKa_3 = 13.41$

$H_3AsO_4 \leftrightarrow H_2AsO_4^- + H^+$ $pKa_1 = 2.24$

$H_2AsO_4^- \leftrightarrow HAsO_4^{2-} + H^+$ $pKa_2 = 6.94$

$HAsO_4^{2-} \leftrightarrow AsO_4^{3-} + H^+$ $pKa_3 = 11.50$

When pH is below the point of zero charge (pH_{PZC}), the surface of adsorbents will form positive charges. At this time, As(V) predominantly exists as $H_2AsO_4^-$ and adsorption occurs by electrostatic and chemical attraction (Cheng et al., 2016). At higher pH values, the major As species exist as $HAsO_4^{2-}$ and AsO_4^{3-}. However, the availability of binding sites declines with increasing pH. When the pH is above the pH_{PZC} adsorbent surfaces develop negative charges, which repulse anions including $HAsO_4^{2-}$ and AsO_4^{3-}. In the meantime, hydroxide ions compete for positively charged surface sites, and as a result weaken the adsorption process (Feng et al., 2015). Furthermore, an early study reported that the properties and mineralogical

composition of RM will be changed by pH and specific sorption locations of RM will decrease with increasing pH (Castaldi et al., 2010).

The adsorbed volume of As(III) reached its maximum between pH 8 to 10 (Fig.3.b). This is consistent with the results obtained by Baig et al. (2014), using magnetic biochar, who noted that As(III) adsorption reached a maximum at pH=8 (Baig et al., 2014). Manju et al. (1998) using copper impregnated activated carbon as a sorbent, also discovered that As(III) adsorption increased with increasing pH (Manju et al., 1998). However, Yu et al. (2015) demonstrated that As(III) reached a maximum at pH=3 with manganese oxide-modified biochar (Yu et al., 2015). This variation may be the result of the diverse adsorbents used in the investigations.

3.3. Adsorption Kinetics

As(V) and As(III) kinetic experiments revealed a rapid initial sorption followed by a smooth increase, reaching equilibrium within less than 24 h (Fig. 4). First-order and second-order models were used to describe mononuclear and binuclear adsorption, whilst the Elovich model considers the influence of desorption (Lǔ et al., 2013). Compared with BC, RM-BC showed a greater sorption capacity for As. Kinetic models and best-fit parameter values for As(V) and As(III) adsorption data are listed in Table 1. The pseudo-second-order model fits the kinetic data well when compared to pseudo-first-order for As(V) adsorption on all adsorbents (Table 1). However, for As(III) adsorption on BC and RM-BC, the fit is different. Between the three kinetic models, the former is more in favor of the pseudo-second-order model.

For the latter, the Elovich model agrees with the data more accurately.

The results revealed that: (1) according to the assumptions of the pseudo-second-order kinetic model, the reaction rate is relative to the amount of BC/RM-BC surface active sites and the rate-limiting step will possibly be chemical sorption (Taty-Costodes et al., 2003; Mohan et al., 2011), (2) the adsorption of As(III) on RM-BC was a heterogeneous process and may be controlled by multiple mechanisms including chemisorption (Yao et al., 2014), and (3) both BC and RM-BC removed As(V) more effectively than As(III). In addition, the adsorption density of As(V) on RM-BC is more than that of BC.

3.4. Adsorption isotherms

Langmuir and Freundlich isotherms for As(V) and As(III) on BC and RM-BC are displayed in Fig. 5. With increasing As concentration, As adsorption increased greatly until reaching equilibrium. In this study, all sorption isotherms were ‘‘L’’ shaped with higher R^2 compared to the Freundlich model (Table 2). The calculated Langmuir maximum adsorption capacity (Q_{max}) of RM-BC for As(V) and As(III) were 5923.8 and 520.0 $ug \cdot g^{-1}$ respectively. In contrast, the Q_{max} of BC for As(V) and As(III) were only 552.0 $ug \cdot g^{-1}$ and 447.6 $ug \cdot g^{-1}$ respectively.

The Langmuir isotherm is used to describe monolayer adsorption on sorbent surfaces (Awwad et al., 2010). Both BC and RM-BC obey the adsorption mechanisms of Langmuir, which is in accordance with many carbonaceous adsorbents (Zhang et al., 2013; Wang et al., 2015a). Red mud-modified biochar exhibited improved

331 removal for As(V) and As(III) compared to BC, suggesting that it may enhance
332 biochar adsorption sites (Wang et al., 2015a; Li et al., 2016).

333 In this work, R_L values for As(V) adsorption on BC and RM-BC and As(III)
334 adsorption on BC and RM-BC were in the range of 0.0663-0.825, 0.303-0.970,
335 0.136-0.919, 0.0778-0.860 respectively, indicating that adsorption was favorable.

336 Table 4 presents a comparison of maximum adsorptive capacities for various As(V)
337 adsorbents. The Langmuir maximum sorption capacity of RM-BC for As(V) is lower
338 than that of Fe coated biochars (Samsuri et al.(2013)) and La loaded biochar (Feng et
339 al. (2015)). Nevertheless, production of biochar treated with pure chemical reagents
340 (Fe and La) would be expensive at an industrial level.

341 *3.5. Analysis of adsorption mechanisms*

342 K-edge XANES analyses for As standards and RM-BC-As(V) are presented in Fig.
343 6. The excitation energies are displayed at 11872.4 eV and 11876.5 eV corresponding
344 to As(III) and As(V) respectively. The results of XANES spectra revealed that both
345 As(V) and As(III) were adsorbed on the surface of the red mud. Arsenate was the
346 major species and accounted for 97.6% of the total As (Table 3). In addition, LCF
347 results revealed three main As phases on RM-BC including hematite-As(V) (53.5%),
348 magnetite-As(V) (33.8%), and gibbsite-As(V) (13.6%), which probably formed
349 during the sorption process (Table 3).

350 Previous studies demonstrated that iron and alumina oxides play a key role in As
351 sorption (Zhang et al., 2014; Wang et al., 2015a). The presence of hematite, goethite,
352 magnetite and gibbsite, as revealed by XRD, on RM-BC is consistent with that

353 reported in other studies (Li et al., 2009; Liu and Naidu, 2014). Arsenate forms inner
354 sphere bidentate binuclear complexes on gibbsite (Ladeira et al., 2001). Hematite,
355 goethite, and magnetite both effectively remove As(III) and As(V) from solutions,
356 especially hematite, as this demonstrated the greatest adsorption capacity in acidic pH
357 conditions (Gimenez et al., 2007; Mamindy-Pajany et al., 2011). Arsenate was
358 strongly bound to iron oxides by forming inner sphere complexes through ligand
359 exchange (Jain et al., 1999; Mamindy-Pajany et al., 2011).

360 According to XANES results, possible adsorption mechanisms for As(V) on
361 RM-BC are presented in Fig.7. The structure M-O-As(V) formed may substantially
362 enhanced the adsorption capacity of As(V). This figure was consistent with previous
363 studies demonstrating that the mechanisms responsible for As adsorption on biochar
364 are through electrostatic interactions, surface complexation through ligand exchange
365 (described as inner-sphere surface monodentate and bidentate complexes), and
366 chemical interactions between As and surface functional groups (Li et al., 2016; Wang
367 et al., 2015a; Zhang et al., 2013).

368 ## 4. Conclusion

369 Red mud and rice straw biochar are promising materials for As contaminated soil
370 remediation due to their improved adsorbent capacity. RM-BC revealed improved
371 removal of both As(V) and As(III), with the maximum adsorption capacity ten times
372 greater than that of the untreated biochar. All sorption isotherms produced improved
373 fits for the Langmuir model. X-ray absorption near-edge spectroscopy indicated that
374 the adsorption of As(V) on RM-BC was possibly due to surface complexation and

electrostatic interactions.

Acknowledgments

Financial supports from China Postdoctoral Science Foundation (2016M590755), Natural Science Foundation of Hunan, China (No. 2015JJ3142) and Teacher's Research Foundation of Central South University are gratefully acknowledged. The authors would also like to thank the Shanghai Synchrotron Radiation Facility for technical assistance, and Mr. Wangyang Zhou and Mr. JingYu Mo in Central South University for assisting various experiments and preparation of the manuscript.

References

Adra, A., Morin, G., Nguema, G.O., Brest, J., 2015. Arsenate and Arsenite Adsorption onto Al-containing ferrihydrites implications for arsenic immobilization after neutralization of acid mine drainage. Appl. Geochem. 64, 2-9.

Ahmad, M., Rajapaksha, A.U., Lim, J.E., Zhang, M., Bolan, N., Mohan, D., Vithanage, M., Lee, S.S., Ok, Y.S., 2014. Biochar as a sorbent for contaminant management in soil and water: A review. Chemosphere. 99, 19-33.

Altundogan, H.S., Altundogan, S., Tumen, F., Bildik, M., 2000. Arsenic removal from aqueous solutions by adsorption on red mud, Waste Manage. 20, 761-767.

Awwad, N.S., Gad, H.M.H., Ahmad, M.I., Aly, H.F., 2010. Sorption of lanthanum and erbium from aqueous solution by activated carbon prepared from rice husk. Colloids Surf., B. 81, 593-599.

Baig, S.A., Zhu, J., Muhammad, N., Sheng, T., Xu, X., 2014. Effect of synthesis methods on magnetic Kans grass biochar for enhanced As(III, V) adsorption from aqueous solutions. Biomass Bioenergy. 71, 299-310.

Beesley, L., Inneh, O.S., Norton, G.J., Moreno-Jimenez, E., Pardo, T., Clemente, R., Dawson, J.J.C., 2014. Assessing the influence of compost and biochar amendments on the mobility and toxicity of metals and arsenic in a naturally contaminated mine soil. Environ. Pollut. 186, 195-202.

Castaldi, P., Silvetti, M., Enzo, S., Melis, P., 2010. Study of sorption processes and FT-IR analysis of arsenate sorbed onto red muds (a bauxite ore processing waste). J. Hazard. Mater. 175, 172-178.

Chang, K., Chen, C., Lin, J., Hsien, J., Wang, Y., Zhao, F., Shih, Y., Xing, Z., Chen, S., 2014. Rice straw-derived activated carbons for the removal of carbofuran from an aqueous solution. New Carbon Mater. 29, 47-54.

Cheng, Q., Huang, Q., Khan, S., Liu, Y., Liao, Z., Li, G., Ok, Y.S., 2016. Adsorption of Cd by peanut

husks and peanut husk biochar from aqueous solutions. Ecol. Eng. 87, 240-245.
Fan, J.X., Wang, Y., Liu, C., Wang, L., Yang, K., Zhou, D., Li, W., Sparks, D.L., 2014. Effect of iron oxide reductive dissolution on the transformation and immobilization of arsenic in soils: New insights from X-ray photoelectron and X-ray absorption spectroscopy. J. Hazard. Mater. 279, 212-219.
Feng, Y., Xue, L., Yang, B., Liu, Y., Duan, J., He, S., Yang, L., 2015. Adsorption of As from aqueous solution by lanthanum oxide-loaded biochar：process and mechanisms. Journal of Agro-Environment Science. 34, 2190-2197.
Genc, H., Tjell, J.C., Mcconchie, D., Schuiling, O., 2003. Adsorption of arsenate from water using neutralized red mud, J. Colloid Interface Sci. 264, 327-334.
Gimenez, J., Martinez, M., Depabio, J., Rovira, M., Duro, L., 2007. Arsenic sorption onto natural hematite, magnetite, and goethite. J. Hazard. Mater. 141, 575-580.
Gregory, S.J., Anderson, C.W.N., Camps Arbestain, M., McManus, M.T., 2014. Response of plant and soil microbes to biochar amendment of an arsenic-contaminated soil. Agriculture, Ecosystems & Environment. 191, 133-141.
Guo, H., Li, Y., Zhao, K., Ren, Y., Wei, C., 2011. Removal of arsenite from water by synthetic siderite: Behaviors and mechanisms. J. Hazard. Mater. 186, 1847-1854.
Hartley, W., Dickinson, N.M., Riby, P., Lepp, N.W., 2009. Arsenic mobility in brownfield soils amended with green waste compost or biochar and planted with Miscanthus. Environ. Pollut. 157, 2654-2662.
Jadhav, S.V., Bringas, E., Yadav, G.D., Rathod, V.K., Ortiz, I., Marathe, K.V., 2015. Arsenic and fluoride contaminated groundwaters: A review of current technologies for contaminants removal. J. Environ. Manage. 162, 306-325.
Jain, A., Raven, K.P., Loeppert, R.H., 1999. Arsenite and arsenate adsorption on ferrihydrite: surface charge reduction and net OH^- release stoichiometry. Environ. Sci. Technol. 33, 1179-1184.
Kim, E.J., Yoo, J., Baek, K., 2014. Arsenic speciation and bioaccessibility in arsenic-contaminated soils: sequential extraction and mineralogical investigation. Environ. Pollut. 186, 29-35.
Klauber, C., Gräfe, M., Power, G., 2011. Bauxite residue issues: II. options for residue utilization. Hydrometallurgy. 108, 11-32.
Ladeira, A.C.Q., Ciminelli, V.S.T., Duarte, H.A., Alves, M.C.M., Ramos, A.Y., 2001. Mechanism of anion retention from EXAFS and density functional calculations: Arsenic (V) adsorbed on gibbsite, Geochimica Et Cosmochimica Acta. 8, 1211-1217.
Lee, S., Kim, E.Y., Park, H., Yun, J., Kim, J., 2011. In situ stabilization of arsenic and metal-contaminated agricultural soil using industrial by-products. Geoderma. 161, 1-7.
Li, R., Wang, J.J., Zhou, B., Awasthi, M.K., Ali, A., Zhang, Z., Gaston, L.A., Lahori, A.H., Mahar, A., 2016. Enhancing phosphate adsorption by Mg/Al layered double hydroxide functionalized biochar with different Mg/Al ratios. Sci. Total Environ. 559, 121-129.
Li, X., Xiao, W., Liu, W., Liu, G., Peng, Z., Zhou, Q., Qi, T., 2009. Recovery of alumina and ferric oxide from Bayer red mud rich in iron by reduction sintering. Trans. Nonferrous Met. Soc. 19, 1342-1347.
Liu, Y., Naidu, R., 2014. Hidden values in bauxite residue (red mud): recovery of metals. Waste Manage. 34, 2662-2673.
Liu, Y., Naidu, R., Ming, H., 2011. Red mud as an amendment for pollutants in solid and liquid phases. Geoderma. 163, 1-12.
Lone, A.H., Najar, G.R., Ganie, M.A., Sofi, J.A., Ali, T., 2015. Biochar for sustainable soil health: a

review of prospects and concerns, Pedosphere. 25, 639-653.
Lopes, G., Guilherme, L.R.G., Costa, E.T.S., Curi, N., Penha, H.G.V., 2013. Increasing arsenic sorption on red mud by phosphogypsum addition. J. Hazard. Mater. 262, 1196-1203.
Lǔ, J., Liu, H., Liu, R., Zhao, X., Sun, L., Qu, J., 2013. Adsorptive removal of phosphate by a nanostructured Fe−Al−Mn trimetal oxide adsorbent. Powder Technol. 233, 146-154.
Mamindy-Pajany, Y., Hurel, C., Marmier, N., Roméo, M., 2011. Arsenic (V) adsorption from aqueous solution onto goethite, hematite, magnetite and zero-valent iron: Effects of pH, concentration and reversibility. Desalination. 281, 93-99.
Manju, G.N., Raji, C., Anirudhan T.S., 1998. Evaluation of coconut husk carbon for the removal of arsenic from water. Water Res. 32, 3062-3070.
Mohan, D., Rajput, S., Singh, V.K., Steele, P.H., Pittman, C.U., 2011. Modeling and evaluation of chromium remediation from water using low cost bio-char, a green adsorbent. J. Hazard. Mater. 188, 319-333.
Rubinos D. A., Arias M., Díaz-Fierros F., Barral1 M. T., 2005. Speciation of adsorbed arsenic(V) on red mud using a sequential extraction procedure. Mineralogical Magazine, 69 (5), 591-600.
Samsuri, A.W., Sadegh-Zadeh, F., Seh-Bardan, B.J., 2013. Adsorption of As(III) and As(V) by Fe coated biochars and biochars produced from empty fruit bunch and rice husk. Journal of Environmental Chemical Engineering, 1, 981-988.
Sun, L., Chen, D., Wan, S., Yu, Z., 2015. Performance, kinetics, and equilibrium of methylene blue adsorption on biochar derived from eucalyptus saw dust modified with citric, tartaric, and acetic acids. Bioresource. Technol. 198, 300-308.
Tan, X., Liu, Y., Gu, Y., Xu, Y., Zeng, G., Hu, X., Liu, S., Wang, X., Liu, S., Li, J., 2016. Biochar-based nano-composites for the decontamination of wastewater: a review. Bioresource. Technol. 212, 318-333.
Taty-Costodes, V.C., Fauduet, H., Porte, C., Delacroix, A., 2003. Removal of Cd(II) and Pb(II) ions, from aqueous solutions by adsorption onto sawdust of Pinus sylvestris. J. Hazard. Mater. 105, 121-142.
Wang, S., Gao, B., Zimmerman, A.R., Li, Y., Ma, L., Harris, W.G., Migliaccio, K.W., 2015a. Removal of arsenic by magnetic biochar prepared from pinewood and natural hematite. Bioresource. Technol. 175, 391-395.
Wang, S., Gao, B., Li, Y., Mosa, A., Zimmerman, A.R., Mab, L.Q. Harris, W.G., Migliaccio, K.W., 2015b. Manganese oxide-modified biochars: Preparation, characterization, and sorption of arsenate and lead. Bioresource. Technol. 181, 13-17.
Wei, Z., Liang, K., Wu, Y., Zou, Y., Zuo, J., Arriagada, D.C., Pan, Z., Hu, G., 2016. The effect of pH on the adsorption of arsenic(III) and arsenic(V) at the TiO_2 anatase [101] surface. J. Colloid Interface Sci. 462, 252-259.
WHO Arsenic and arsenic compounds. Environmental health criteria 224; World Health Organization: Geneva, Switzerland, 2001
Wu, C., Zou, Q., Xue, S., Pan, W., Huang, L., Hartley, W., Mo, J.Y., Wong, M., 2016a. The effect of silicon on iron plaque formation and arsenic accumulation in rice genotypes with different radial oxygen loss (ROL). Environ. Pollut. 212, 27-33.
Wu, C., Huang, L., Xue, S.G., Qin, Z., Shi, L.Z., 2016b. Review on application of bauxite residue on As comtamination remediation. Environmental Chemistry. 35, 141-149.
Xia, D., Tan, F., Jiang, C.Z, Chen X.Z., Li, H., Zheng, Y., Li, Q., Wang, Y., 2016. $ZnCl_2$-activated biochar from biogas residue facilitates, appl. surf. Sci. 377, 361-369.

Yan, X.L., Lin, L.Y., Liao, X.Y., Zhang, W.B., Wen, Y., 2013. Arsenic stabilization by zero-valent iron, bauxite residue, and zeolite at a contaminated site planting Panax notoginseng. Chemosphere, 93, 661-667.

Yao, Y., Gao, B., Fang, J., Zhang, M., Chen, H., Zhou, Y., Creamer, A.E., Sun, Y., Yang, L., 2014. Characterization and environmental applications of clay-biochar composites. Chem. Eng. J. 242, 136-143.

Yu Z.H., Huang, Y., Lian, F., Xie, L., LIU, S. Song, Z., 2015. Adsorption of Arsenic（Ⅲ）on biochar-manganese oxide composites, Journal of Agro-Environment Science. 1, 155-161.

Zhang, M., Gao, B., Varnoosfaderani, S., Hebard, A., Yao, Y., Inyang, M., 2013. Preparation and characterization of a novel magnetic biochar for arsenic removal. Bioresource. Technol. 130, 457-462.

Zhang, G., Liu, F., Liu, H., Qu, J., Liu, R., 2014. Respective role of Fe and Mn oxide contents for arsenic sorption in iron and manganese binary oxide: an x-ray absorption spectroscopy investigation. Environ. Sci. Technol. 48, 10316-10322.

Zhang, X., Sarmah, A.K., Bolan, N.S., He, L., Lin, X., Che, L., Tang, C., Wang, H., 2016. Effect of aging process on adsorption of diethyl phthalate in soils amended with bamboo biochar. Chemosphere, 142, 28-34.

526 **Table 1** Kinetic models and best-fit parameters for As(V) and As(III) adsorption data.

sample		First-order			Second-order			Elovich			Intraparticle diffusion		
		$k_1(h^{-1})$	$q_e(\mu g/g)$	R^2	$k_2(g\ \mu g^{-1}\ h^{-1})$	$q_e(\mu g/g)$	R^2	$\beta(\mu g/g)$	$\alpha(\mu g/g)$	R^2	$K_d(\mu g\ g^{-1}\ min^{-1/2})$	$C(\mu g/g)$	R^2
BC	As(V)	1.195	451.4	0.983	0.00357	482.9	0.987	0.0143	4168.5	0.884	62.96	233.1	0.6664
RM-BC	As(V)	1.446	1656.5	0.900	0.00126	1758.6	0.957	0.00435	31085.8	0.917	212.94	908.7	0.7298
BC	As(III)	0.805	296.0	0.948	0.00366	319.5	0.960	0.0190	1196.7	0.928	48.95	115.1	0.7662
RM-BC	As(III)	0.686	377.9	0.911	0.00236	412.0	0.927	0.0144	1253.1	0.962	66.57	132.9	0.8842

527

528

Table 2 Isotherm models and best-fit parameters for As(V) and As(III) adsorption data.

sample		Langmuir			Freundlich		
		$k(\mu g^{-1})$	Q_{max} (μg/g)	R^2	$k(\mu g^{(1-n)} L^n g^{-1})$	n	R^2
BC	As(V)	0.296	552.0	0.949	179.2	0.293	0.786
RM-BC	As(V)	0.0465	5923.8	0.997	452.9	0.579	0.985
BC	As(III)	0.179	447.6	0.991	119.9	0.401	0.898
RM-BC	As(III)	0.333	520.0	0.995	171.2	0.312	0.911

548 **Table 3** SPOIL values of reference materials obtained by target transformation (TT), and linear

549 combination fit (LCF) results of As(V) adsorption on RM-BC.

References	SPOIL Values		LCF results(%)
	Spoil	R	RM-As(V)
As(III)	0	0.01865	2.4
As(V)	0.3172	0.02239	97.6
R-factor			0.00868
Chi-square			0.0697
gibbsite-As(V)	0	9.16E-07	13.6
hematite-As(V)	0	1.37E-07	53.5
magnetite-As(V)	1.0423	5.61E-05	33.8
R-factor			0.00241
Chi-square			0.193

550

551

552

553

554

555

556

557

558

559

560

561

562

563

564

565 **Table 4** Comparison of adsorption capabilities for different adsorbents of As(V).

Adsorbents	**Feedstock**	**q_{max}(μg/g)**	**References**
red mud modified biochar	rice straw	5923.8	This work
hematite modified biochar	loblolly pine(*Pinus taeda*) wood	428.7	Wang et al.(2015a)
$MnCl_2 \cdot 4H_2O$ modified biochar	pine wood	590	Wang et al.(2015b)
birnessite modified biochar	pine wood	910	Wang et al.(2015b)
Fe coated biochars	empty fruit bunch	15200	Samsuri et al.(2013)
Fe coated biochars	rice husk	16900	Samsuri et al.(2013)
La loaded Biochar	corn stalk	38020	Feng et al. (2015)
Red mud	——	941	Altundogan et al. (2000)

566

567

568

569

570

571

572

573

574

575

576

577

578

579

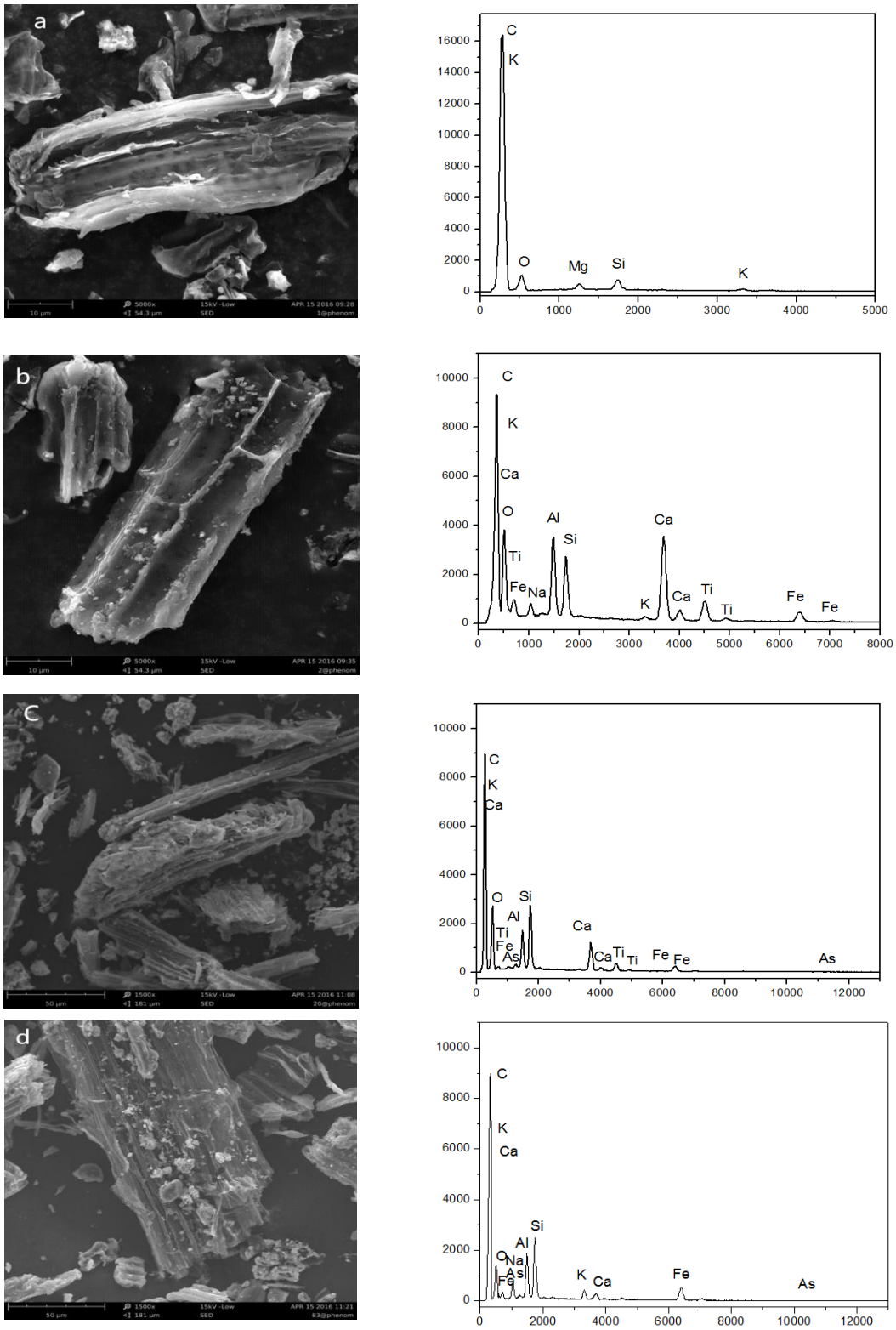

Fig. 1. SEM-EDS of biochar (BC) and red mud-modified biochar (RM-BC): a. BC, b. RM-BC before adsorption; c. RM-BC after adsorption of As(V), d. RM-BC after adsorption of As(III).

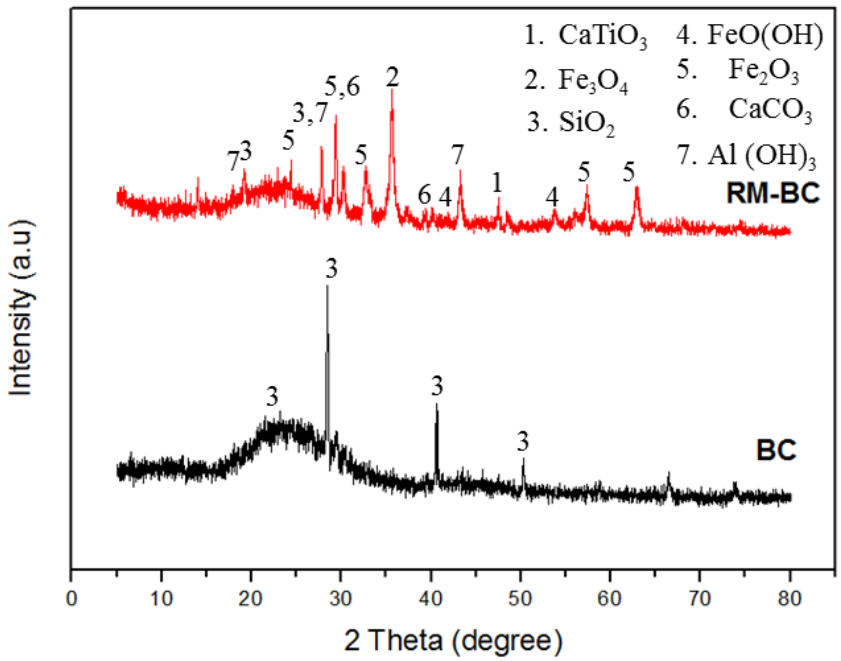

Fig. 2. X-ray diffraction spectra of biochar (BC) and red mud-modified biochar (RM-BC).

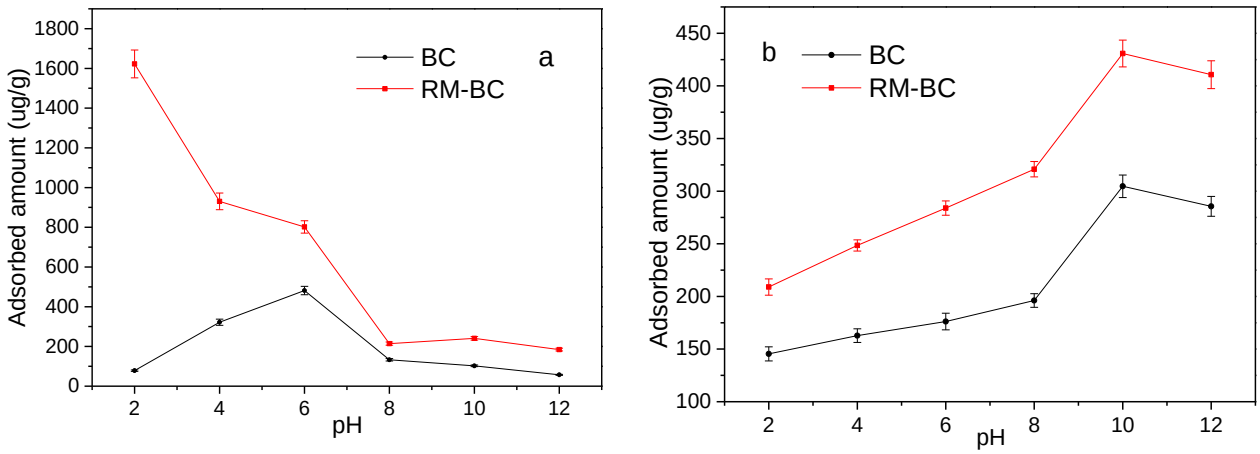

598 **Fig. 3.** Effect of pH on the concentration of (a) As(V) and (b) As(III) adsorbed by BC and

599 RM-BC.

600

601

602

603

604

605

606

607

608

609

610

611

612

613

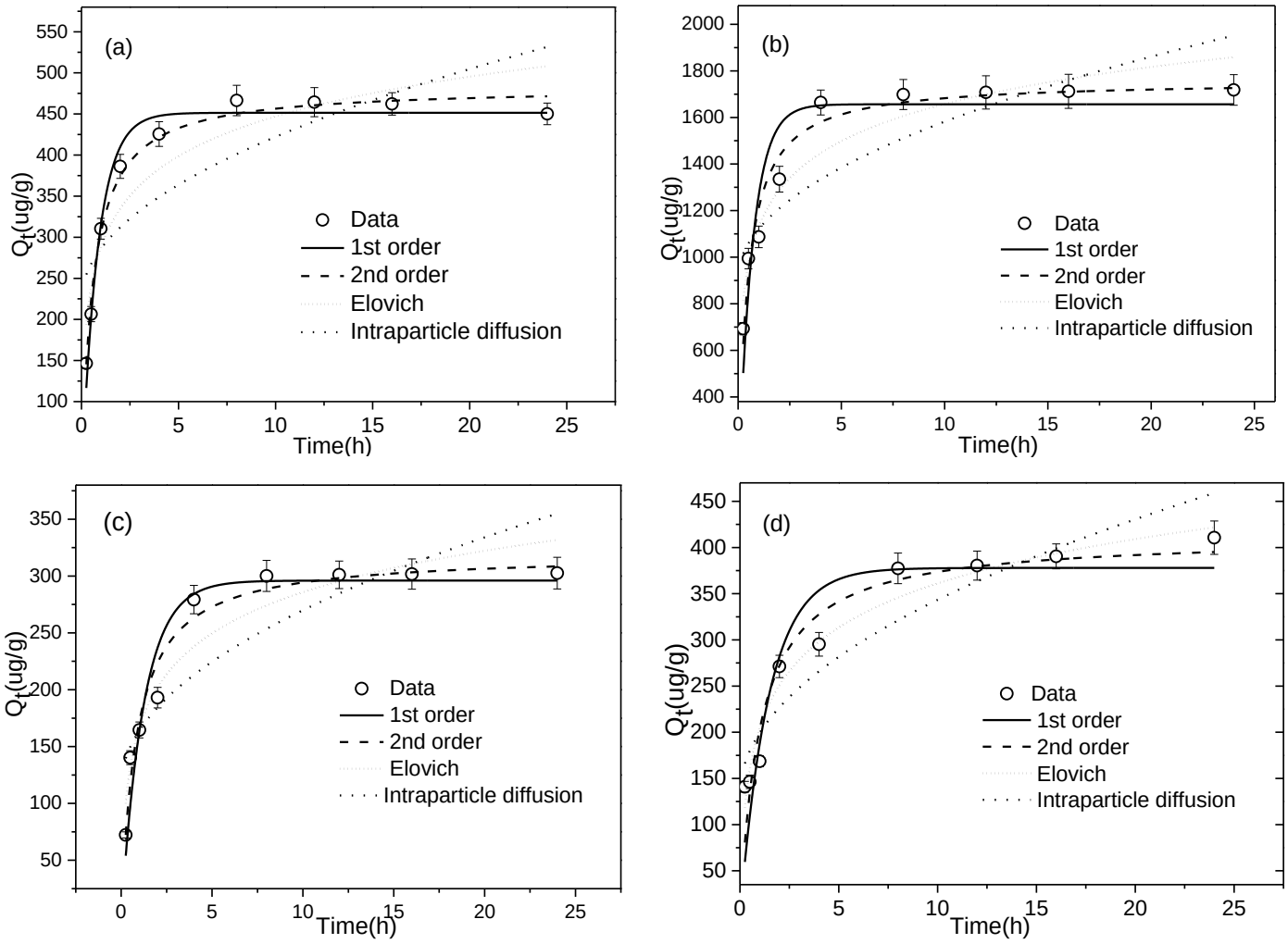

Fig. 4. Adsorption kinetics and modeling for As on adsorbents: (a) and (b) are As(V) adsorption on BC and RM-BC respectively. (c) and (d) are As(III) adsorption on BC and RM-BC respectively.

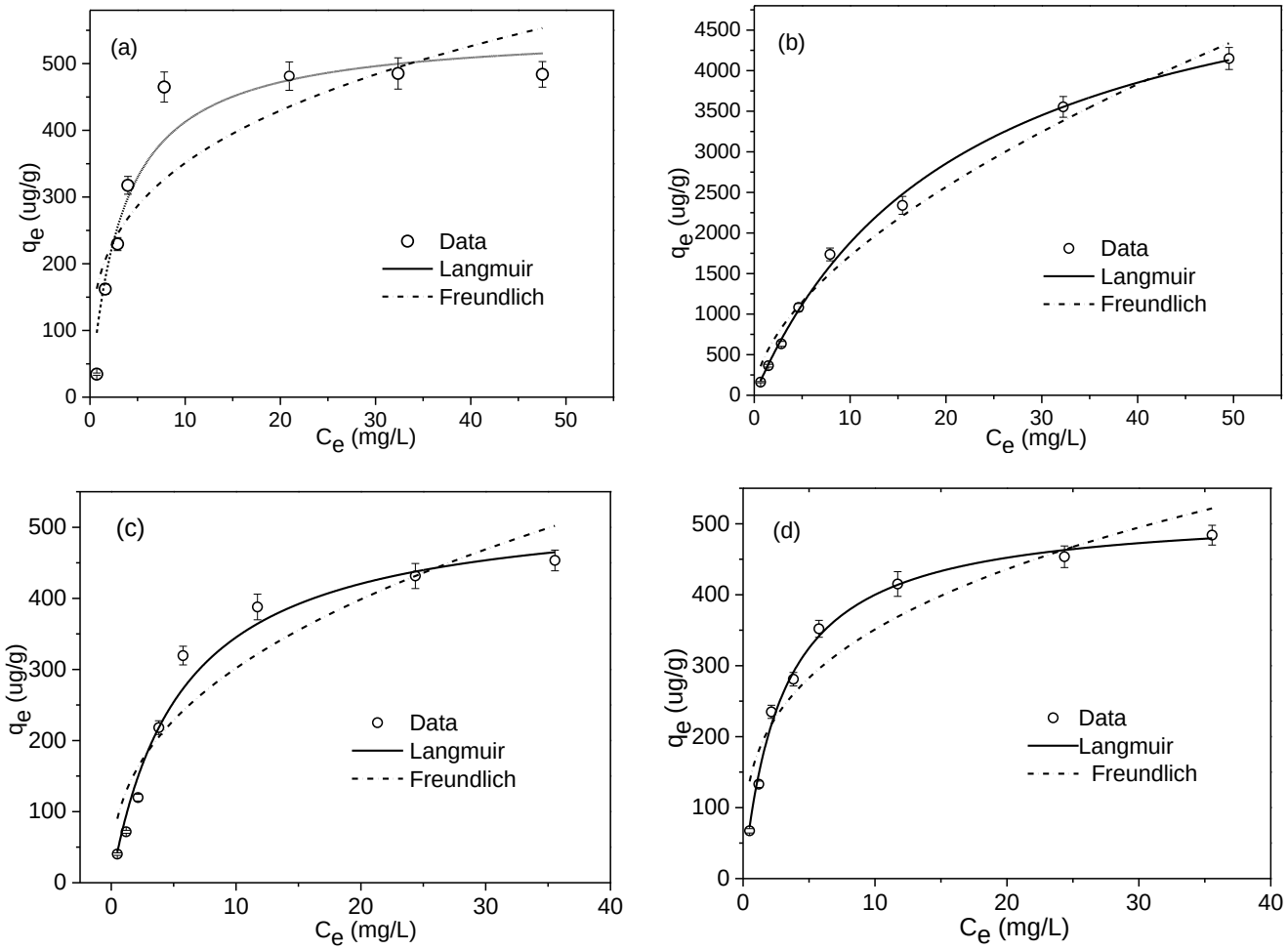

Fig. 5. Adsorption isotherm data and modeling for As on adsorbents: (a) and (b) are As(V) adsorption on BC and RM-BC respectively. (c) and (d) are As(III) adsorption on BC and RM-BC respectively.

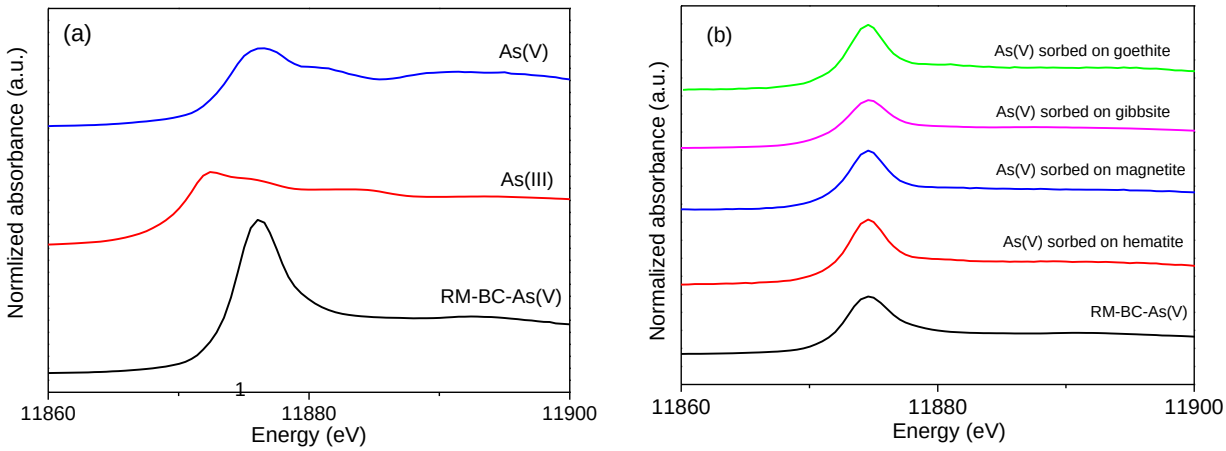

631 **Fig. 6.** Normalized As k-edge X-ray absorption near-edge structure (XANES) spectra for As(V)
632 adsorption on RM-BC (a) the percentages of As species; (b) the percentages of As adsorbed on
633 different minerals; All fit parameters are detailed in Table 3.

634
635
636
637
638
639
640
641
642
643
644
645
646
647
648
649
650
651
652
653
654
655
656
657

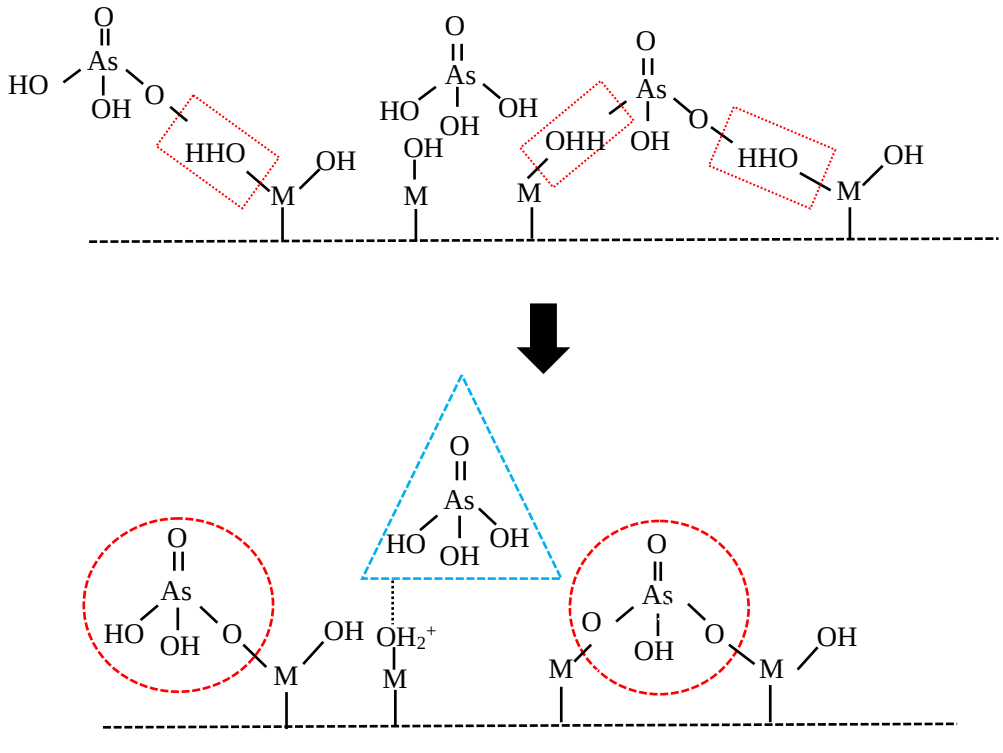

Fig. 7. Mechanism of As(V) adsorption on red mud-modified biochar, where M is the metal oxide composition of the red mud surface.

693 **Table and figure legends**

694 **Table 1** Kinetic models and best-fit parameter values for As(V) and As(III) adsorption data.

695 **Table 2** Isotherm models and best-fit parameter values for As(V) and As(III) adsorption data.

696 **Table 3** SPOIL values of references obtained by target transformation (TT), and linear
697 combination fit (LCF) results of As(V) adsorption on RM-BC.

698 **Table 4** Comparison of the adsorption capacities of different adsorbents for As(V).

699 **Fig. 1.** SEM-EDS of biochar (BC) and red mud-modified biochar (RM-BC): a. BC, b. RM-BC
700 before adsorption; c. RM-BC after adsorption of As(V), d. RM-BC after adsorption of As(III).

701 **Fig. 2.** X-ray diffraction spectra of biochar (BC) and red mud-modified biochar (RM-BC).

702 **Fig. 3.** Effect of pH on the concentration of (a) As(V) and (b) As(III) adsorbed by BC and
703 RM-BC.

704 **Fig. 4.** Adsorption kinetics and modeling for As onto adsorbents: (a) and (b) are As(V)
705 adsorption on BC and RM-BC respectively. (c) and (d) are As(III) adsorption on BC and RM-BC
706 respectively.

707 **Fig. 5.** Adsorption isotherm data and modeling for As onto adsorbents: (a) and (b) are As(V)
708 adsorption on BC and RM-BC respectively. (c) and (d) are As(III) adsorption on BC and
709 RM-BC respectively.

710 **Fig. 6.** Normalized As k-edge X-ray absorption near-edge structure (XANES) spectra for As(V)
711 adsorption on RM-BC (a) the percentages of As species; (b) the percentages of As adsorbed on
712 different minerals; All fit parameters are detailed in Table 3.

713 **Fig. 7.** Mechanism of As(V) adsorption on red mud-modified biochar, where M is the metal
714 oxide composition of the red mud surface.

715